PROCEEDINGS OF SCIENCE

B-physics observables in the continuum from a combination of static and relativistic results

Alessandro Conigli,[mz,g] **Julien Frison,**[n] **Patrick Fritzsch,**[d] **Antoine Gérardin,**[mar] **Jochen Heitger,**[mu] **Gregorio Herdoiza,**[ma] **Simon Kuberski,**[c] **Carlos Pena**[ma] **and Hubert Simma**[n]

[n] *John von Neumann-Institut für Computing NIC, Deutsches Elektronen-Synchrotron DESY, Platanenallee 6, 15738 Zeuthen, Germany*

[ma] *Instituto de Física Teórica UAM-CSIC and Dpto. de Física Teórica C/ Nicolás Cabrera 13-15, Universidad Autónoma de Madrid, Cantoblanco E-28049 Madrid, Spain*

[mu] *Universität Münster, Institut für Theoretische Physik, Wilhelm-Klemm-Straße 9, 48149 Münster, Germany*

[mar] *Aix-Marseille Université, Université de Toulon, CNRS, CPT, Marseille, France*

[d] *School of Mathematics, Trinity College Dublin, Dublin 2, Ireland*

[c] *Theoretical Physics Department, CERN, 1211 Geneva 23, Switzerland*

[mz] *Helmholtz Institute Mainz, Johannes Gutenberg University, Mainz, Germany*

[g] *GSI Helmholtz Centre for Heavy Ion Research, Darmstadt, Germany*

E-mail: aconigli@uni-mainz.de

We discuss how to perform interpolations between relativistic and static computations in order to extract heavy-light B-physics observables in the continuum. This strategy can be carried out entirely in large volume, but its predictivity is enhanced by the following step scaling approach. Relativistic computations are carried out at the physical b-quark mass using the Schrödinger Functional in a box, where small am is accessible. They are connected to large volume observables through step scaling functions that trace the mass dependence between the physical charm region and the static limit, such that B-physics results can be obtained by interpolation. We discuss the extraction of relativistic large volume observables entering the computation, focusing on leptonic and semi-leptonic transition amplitudes. We review in detail our numerical results first presented in [1] for leptonic decays from CLS $N_f = 2 + 1$ ensembles at $m_u = m_d = m_s$, and with five values of the lattice spacing down to 0.039 fm .

European network for Particle physics, Lattice field theory and Extreme computing (EuroPLEx2023)
11-15 September 2023
Berlin, Germany

PoS(EuroPLEx2023)005

1. Introduction

B-physics is a potential gateway to discovering new phenomena beyond the Standard Model (SM), making precise determinations of heavy quark observables essential. The presence of small discrepancies between the SM and experimental measurements is intriguing, but not solid enough to unveil new physics, and a better control of theoretical results is required. As a matter of fact, perturbation theory is not fully reliable at the scale of interest, while non-perturbative approaches based on Lattice QCD calculations suffer from the large ratio between the b quark mass and the $\Lambda_{\rm QCD}$ scale, thus requiring various approximations such as extrapolating to the b-scale to circumvent the issue.

A step forward was made in [2] by combining Step Scaling Functions (SSFs) in the static approximation [3, 4] with the relativistic ones at finite heavy quark mass m_h [5, 6], where the available lattice spacings require $m_h \leq m_b/2$ to avoid the $am_h > 1$ regime. We have further developed this original proposal in [7] by showing how to generalise the strategy to the extraction of semi-leptonic decays, and we presented in [1] preliminary results for the b-quark mass and the $B^{(\star)}$ meson decay constants. Our prescription relies on building suitable quantities with a continuum limit and simple behaviour in $1/m_h$, such that the renormalisation and matching factor in the static theory cancel completely. This basic requirement for a combination of static and relativistic results allows us to interpolate to the physical b-quark scale while controlling the systematics and the cutoff effects involved in B-physics computations on the lattice.

2. Strategy of the computation

The design principle of our approach, detailed in [1, 7] consists in reaching the b-quark scale by interpolation through a combination of static and relativistic results in the continuum. The difficulty in the straight forward application is that the matching of the static theory to QCD introduces mass-dependent matching functions $C_x(m_h^{\rm RGI}/\Lambda)$ that diverge logarithmically in the static limit. Here we avoid these functions by building convenient quantities that cancel them exactly. The general strategy relies only on a combination of static and relativistic results with a linear $1/m_h$ behaviour, instead of focusing on the $1/m_h$ expansion of finite volume effects and step scaling. The above guidelines replace the original idea of [6], namely that one computes small finite volume effects by step scaling. The latter would require to keep physical kinematics in the finite volume, thus making semi-leptonics computations particularly difficult [8].

By cancelling the log-divergent matching functions through suitable combinations, we also loose the absolute normalisation, required to compute and compare with experiments observables such as the CKM matrix element $|V_{ub}|$ and the $B^{(\star)}$ meson decay constants. A workaround is provided by the step scaling approach of [2], where finite volume computations down to a volume size of $L_1 \approx 0.5$ fm give access to fine enough lattice spacings to resolve the relativistic b-quark while keeping $am_b \ll 1$. In this context, the matching factors $C_x(m_h^{\rm RGI}/\Lambda)$ are replaced by a direct relativistic computation, eventually evolved to large volume through step scaling. This approach however requires a non-perturbative proxy for the quark masses in finite volume. In practice, the heavy quark masses are traded for the pseudo-scalar masses $m_B(L)$ in finite volume, defined as in [2] such that they satisfy $\lim_{L\to\infty} m_B(L) = m_B$. The finite-size dependence of $m_B(L)$ can be

determined from the large volume input $y_B = L_{\text{ref}} m_B$ through the chain [7]

$$y_B = L_{\text{ref}} m_B(L_1) + \sigma_m(u_1, y_2) + \rho_m(u_2, y_B), \tag{1}$$

with L_{ref} some reference scale to make observable dimensionless, while σ_m and ρ_m are the SSFs

$$\sigma_m(u_1, y_2) = L_{\text{ref}}\big[m_B(L_2) - m_B(L_1)\big]_{\mathcal{S}_0}, \qquad \rho_m(u_2, y_B) = L_{\text{ref}}\big[(m_B)_{\mathcal{S}_m} - (m_B(L_2))_{\mathcal{S}_0}\big]. \tag{2}$$

Here $\mathcal{S}_m$ and $\mathcal{S}_0$ denote the massive and massless Lines of Constant Physics (LCP) as defined in [7]. The b-quark mass proxies y_i are obtained recursively from the large volume physical input

$$y_B = L_{\text{ref}} m_B, \qquad y_2 = y_B - \rho_m(y_B, u_2), \qquad y_1 = y_2 - \sigma_m(y_2, u_1), \tag{3}$$

where we make use of the running coupling $u_i = \bar{g}^2(L_i)$ of [9, 10] to express the different volumes of size L_i. Eventually, we note that in L_1 the small lattice spacings granting access to the relativistic b-quark mass together with a non-perturbative quark mass renormalisation [11], allow to compute in the continuum

$$\pi_m(u_1, y) = \frac{m_B(L_1)}{m_b^{\text{RGI}}}, \tag{4}$$

connecting the Renormalisation Group Invariant (RGI) quark mass to the heavy-light pseudo-scalar mass $m_B(L_1)$. Therefore, we can rephrase Eq. (1) as

$$m_b^{\text{RGI}} = \frac{1}{L_{\text{ref}}} \frac{y_B - \rho_m(u_2, y_B) - \sigma_m(u_1, y_2)}{\pi_m(u_1, y_1)}. \tag{5}$$

Whereas a detailed study to estimate the systematics is required, we presented in [1] preliminary results for the b-quark mass using the strategy depicted above, finding good agreements with the literature [12].

The above methodology can be easily extended to transition amplitudes: by defining the infinite and finite volume observables as the logarithm of the relevant matrix elements made dimensionless with L_{ref}

$$\Phi_{A_0(\vec{V})}(u, y) = \ln\left(\frac{L_{\text{ref}}^{3/2}}{\sqrt{2}} \hat{f}_{B^{(\star)}}\right), \qquad \hat{f}_{B^{(\star)}} = \sqrt{m_{B^{(\star)}}} f_{B^{(\star)}}, \tag{6}$$

with A_0, $\vec{V}$ denoting the axial and vector heavy-light currents respectively, we obtain a step scaling chain identical in form to Eq. (1), namely [7]

$$\Phi_{A_0(\vec{V})}(y_B) = \Phi_{A_0(\vec{V})}(u_1, y_1) + \sigma_{A_0(\vec{V})}(u_1, y_2) + \rho_{A_0(\vec{V})}(u_2, y_B), \tag{7}$$

with $\sigma_{A_0(\vec{V})}$, $\rho_{A_0(\vec{V})}$ the SSFs

$$\begin{aligned} \sigma_{A_0(\vec{V})}(u_1, y) &= \Phi_{A_0(\vec{V})}(u_2, y) - \Phi_{A_0(\vec{V})}(u_1, y), \\ \rho_{A_0(\vec{V})}(u_2, y) &= \Phi_{A_0(\vec{V})}(y) - \Phi_{A_0(\vec{V})}(u_2, y). \end{aligned} \tag{8}$$

Preliminary results for $f_{B^{(\star)}}$ where presented in [1], and additional details on the various steps of the computation will be given in Section 4. Finally, we stress out that the vector meson decay constant $f_{B^\star}$ is likely to play a crucial role in the extraction of the $B \to \pi \ell \nu$ form factors, as explained in [7]. Indeed, we can push the computation of the form factors with physical kinematics in the large volume only by using the results for the $f_{B^\star}$ SSFs. This allows for a precise determination of the semi-leptonic transition while controlling the systematics involved in the computation.

id	β	a [fm]	L/a	T/a	MDU	$m_\pi L$	L [fm]	N_{m_h}	$m_h^{\max}$
H101	3.40	0.0849(9)	32	96	8064	5.8	2.7	6	$2.5m_c$
B450	3.46	0.0749(8)	32	64	6448	5.1	2.4	6	$2.5m_c$
N202	3.55	0.0633(7)	48	128	7608	6.5	3.0	5	$2.5m_c$
N300	3.70	0.0491(5)	48	128	6160	5.1	2.4	5	$2.5m_c$
J500	3.85	0.0385(4)	64	192	15000	5.2	2.5	5	$2.5m_c$

Table 1: Summary of the $SU(3)$ CLS ensembles employed in this work. The lattice spacing a in physical units taken from [18], the lattice dimension, the length of the Monte Carlo chain in Molecular Dynamics Units (MDU). Approximate values of the product $m_\pi L$ and and the physical extent of the lattice are provided. N_{m_h} refers to the number of measured relativistic heavy quark masses, while $m_h^{\max}$ stands for the heaviest measured mass in units of the charm quark mass m_c.

3. Large volume relativistic observables

In the large volume sector we employ CLS $N_f = 2 + 1$ ensembles [13–16] with non-perturbatively $O(a)$-improved Wilson fermions at the $SU(3)$ symmetric point with $m_\pi = m_K \approx 415$ MeV [17] and five values of the lattice spacing in the range 0.039 fm $< a < 0.087$ fm. A summary of the ensembles employed in the computation is given in Table 1.

We measured relativistic two and three-point correlation functions at multiple heavy quark masses ranging approximately from the charm region m_c and up to $2.5m_c$. The tuning of the charm quark mass was performed combining our expertise from previous works [19, 20]. In the measurements of the three-point correlators we fix the sink as pseudoscalar operator and we vary the ingoing interpolating field and the source operator over the possible gamma structures. A sketch of the computation is given in Fig. 1. The heavy meson and the light spectator momenta are fixed to zero, while non-zero momentum in the range $|\vec{p}| \approx 0, 0.5, 0.8$ GeV is injected in the final light meson. Overall we measured the three-point functions at five different source sink separations ranging from 1.2 fm to 2.8 fm in all the ensembles listed in Tab. 1. We estimate the source and sink position by imposing that $(t_{\text{src}} + t_{\text{snk}})/2$ falls in the center of the lattice for the largest value of t_{snk} taken into account on each ensemble, such that the distance from the boundaries is maximised.

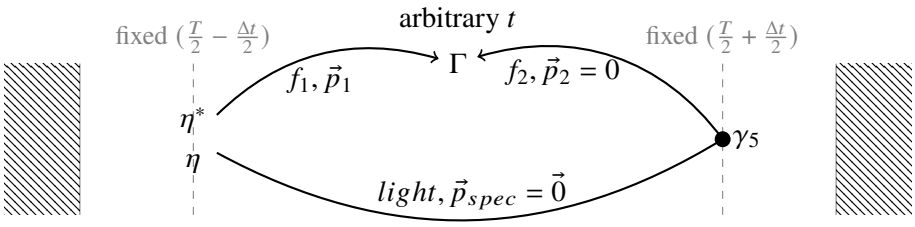

Figure 1: Sketch of the three-point functions computation for the decay of a relativistic heavy mesons f_2 to a light meson f_1. The heavy meson momentum $\vec{p}_2$ and the light spectator momentum $\vec{p}_{\text{spec}}$ are fixed to zero, while non-zero momentum is injected in the final light meson $\vec{p}_1$.

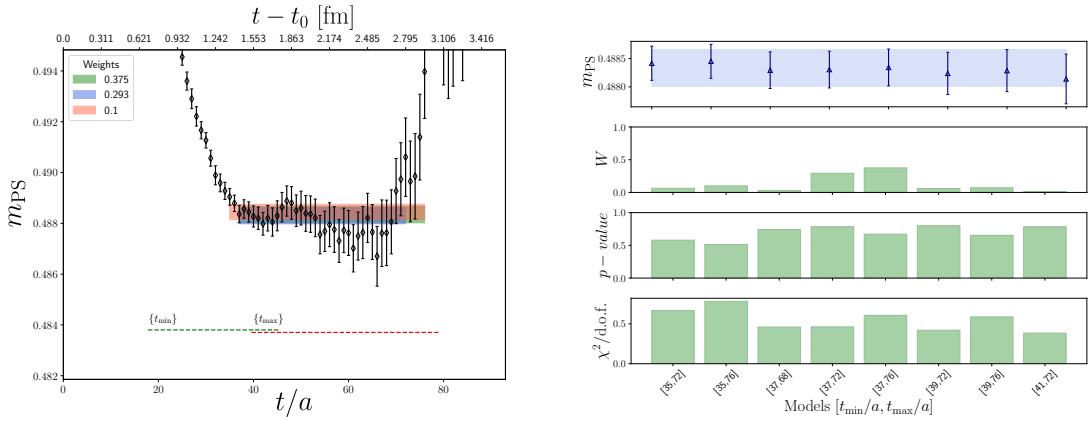

Figure 2: Illustration of the ground state extraction for the reference ensemble J500. *Left*: Effective mass for an heavy-light pseudo-scalar meson with the three fits with higher weight according to our model average prescription. The green and red dashed lines denote the explored fit ranges in Euclidean time for $t_{\rm min}$ and $t_{\rm max}$ respectively. *Right:* Summary of the fit results over different intervals together with the corresponding weights given by the IC prescription. p-values and χ^2/d.o.f.. The shaded blue band in the upper panel corresponds to the model average result.

3.1 Meson masses

In our strategy heavy-light meson masses are used to define the y_i introduced in Eq. (3), used as proxies for the b-quark mass in the different steps of the computation, and entering also the analysis of leptonic and semi-leptonic decays. As a result, an accurate determination of these quantities is crucial to hit the b-quark scale with great precision. In the relativistic large volume sector we extract ground state meson masses by averaging over the plateau region the effective mass defined in terms of the pseudoscalar correlator $C_{\rm PP}$

$$am_{\rm eff}(x_0) = \log\left(\frac{C_{PP}(x_0, y_0)}{C_{PP}(x_0 + a, y_0)}\right). \tag{9}$$

In Fig. 2 we show an illustration of the heavy-light pseudo-scalar meson plateau extraction for a reference ensemble. In order to determine the optimal fit window we perform several fits to a constant by varying the time ranges of the fitting interval and we then assign a weight to each fit by mean of the Information Criteria (IC) proposed in [21], based on the expectation value of the χ^2 as introduced in [22]. Eventually we perform a weighted model average following the prescription of [23] to arrive at a final result and estimate the systematics arising from the model selection.

3.2 Leptonic decay constants

The extraction of vector leptonic decays in the b-quark region, besides the interest for a new lattice result of the latter, is likely to play a crucial role in a precise determination of $b \to u$ semi-leptonic decays, as discussed in greater detail in [7]. On the other hand, the B-meson pseudo-scalar decay constant serves as a validation of our strategy, as it provides a valid crosscheck with the existing results in the literature [12].

In the context of relativistic large volume, given the $O(a)$-improved axial-vector and vector heavy-light currents A_μ, V_μ, we define the corresponding bare decay constants as

$$f_{\rm PS}^{\rm bare} = \sqrt{\frac{2}{m_{\rm PS}}}|\langle 0|\, A_0\, |{\rm PS}\rangle|, \qquad \epsilon_k f_{\rm V}^{\rm bare} = \sqrt{\frac{2}{m_{\rm V}}}|\langle 0|\, V_k\, |{\rm V}\rangle|, \tag{10}$$

where the states $|{\rm PS}\rangle$ and $|{\rm V}\rangle$ are the ground state of a pseudo-scalar and vector meson, respectively, while ϵ_k denotes the three different polarisations of the vector current. In practice, we extract the relevant matrix elements that mediate the weak transition from suitable combination of pseudo-scalar and vector two-point correlation functions, namely

$$|\langle 0|\, A_0\, |{\rm PS}\rangle| = \sqrt{C_{A_0A_0}(x_0,y_0)}e^{m_{\rm PS}/2(x_0-y_0)}, \qquad |\langle 0|\, V_k\, |{\rm V}\rangle| = \sqrt{C_{V_kV_k}(x_0,y_0)}e^{m_{\rm V}/2(x_0-y_0)}. \tag{11}$$

Eventually, we define the renormalised and improved decay constants as

$$\begin{aligned} f_{\rm PS}^{\rm R} &= Z_A\left[1 + b_A a m_h + \bar{b}_A a\,{\rm tr}\, M_q\right] f_{\rm PS}^{\rm bare} \\ f_{\rm V}^{\rm R} &= Z_V\left[1 + b_V a m_h + \bar{b}_V a\,{\rm tr}\, M_q\right] f_{\rm V}^{\rm bare}, \end{aligned} \tag{12}$$

where m_h is the bare subtracted quark mass and M_q denotes the sea quark mass matrix. The renormalisation constants Z_A and Z_V are taken from the L_2-LCP non-perturbative computation in the Schrödinger Functional chirally rotated setup [24]. The mass-dependent coefficient b_A is taken from the perturbative calculation [25], while we use the non-perturbative determination in [26] for b_V. Finally, $\bar{b}_A$ and $\bar{b}_V$ are neglected, as they are suppressed by the fourth power of the coupling and proportional to the trace of the sea quark mass matrix, where only light quarks enter.

When extracting the decay constant through Eq. (11), we expect the ground state amplitude to govern the large distance behaviour of the effective matrix element, where excited state contributions are by far subleading. Therefore, in order to estimate the optimal plateau region we follow a similar strategy as for the meson masses, by considering multiple fit intervals and applying the model average prescription. An example of the procedure is summarised in Fig. 3, where we show a representative plateau for the pseudo-scalar and vector meson decay constants.

3.3 Semi-leptonic form factors

An accurate knowledge of the form factors for $B \to \pi\ell\nu$ is essential to provide insights for indirect searches of new physics phenomena and to test SM predictions. Following the convention of [27, 28] for the kinematic variables in the HQET basis and working in the rest frame of the heavy B-meson, the amplitude governing the $B \to \pi\ell\nu$ transition admits the following decomposition

$$\begin{aligned} h_\parallel(E_\pi) &= Z_V(2m_B)^{-1/2}\,\langle\pi(p_\pi)|\, V_0(0)\,|B(0)\rangle\,, \\ p_\pi^k h_\perp(E_\pi) &= Z_V(2m_B)^{-1/2}\,\langle\pi(p_\pi)|\, V_k(0)\,|B(0)\rangle\,, \end{aligned} \tag{13}$$

in terms of the two form factors $h_\parallel$, $h_\perp$. This convention is particularly beneficial as the form factors admit an HQET expansion without terms that involve a power of the quark mass, but rather a logarithmic dependence on the mass of the heavy quark arising from the HQET-QCD matching coefficient [27]. The latter can be cancelled in the static theory by considering convenient quantities that admit a simple behaviour in $1/m_h$, such that they can be interpolated in this variable [7].

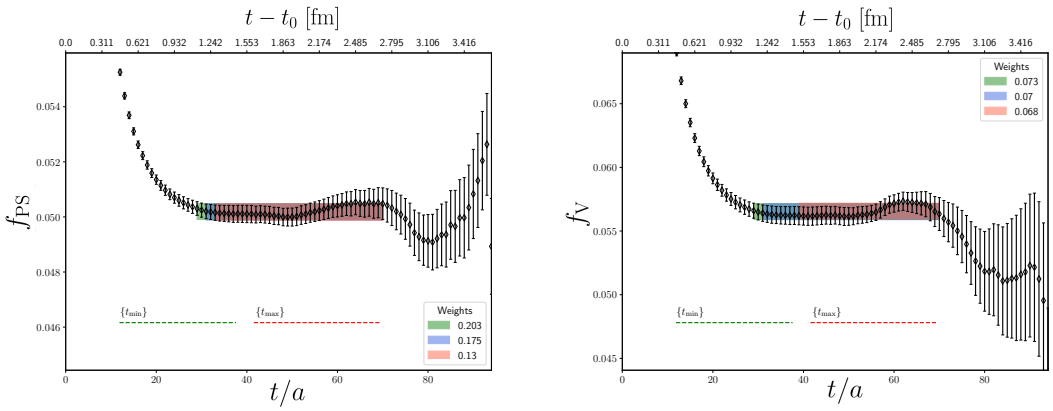

Figure 3: Illustration of plateau extraction for pseudo-scalar (*left*) and vector (*right*) meson decay constants from our model average prescription. The coloured bands represent the three fits with higher weights as assigned from the IC used in this work.

In the context of relativistic large volume, in order to extract the relevant matrix elements we find convenient using suitable combination of two- and three-point functions, such that the dependence on other parameters mostly cancels in the large time limit. To this end we define the ratio [29]

$$\mathcal{R}^{\rm I}_{\mu}(\mathbf{p}_\pi; t, t_s) = \sqrt{2E_\pi}\,\frac{C^{B\to\pi}_{\mu}(\mathbf{p}_\pi; t, t_s)}{\sqrt{C_B(\mathbf{0}; t_{\rm s} - t)C_\pi(\mathbf{p}_\pi; t)}}\sqrt{e^{E_\pi t + m_B(t_s - t)}}, \tag{14}$$

where t_s denotes the separation between the source and the sink in Euclidean time, while $t \leq t_s$ indicates the interval between the source and the inserted current. Another possibility is to consider the double ratio [30]

$$\mathcal{R}^{\rm II}_{\mu}(\mathbf{p}_\pi; t, t_s) = \sqrt{4E_\pi E_B\,\frac{C^{B\to\pi}_{\mu}(\mathbf{p}_\pi; t, t_s)C^{B\to\pi}_{\mu}(\mathbf{p}_\pi; t_s, t)}{C_B(\mathbf{0}; t_s)C_\pi(\mathbf{p}_\pi; t_s)}}. \tag{15}$$

By construction these ratios fulfil

$$\begin{aligned} h_{\parallel}(E_\pi) &= Z_V(2m_B)^{-1/2}\lim_{t_{\rm src}\ll t\ll t_s}\mathcal{R}^{\rm I(II)}_0(\mathbf{p}_\pi; t, t_s), \\ p^k_\pi h_{\perp}(E_\pi) &= Z_V(2m_B)^{-1/2}\lim_{t_{\rm src}\ll t\ll t_s}\mathcal{R}^{\rm I(II)}_k(\mathbf{p}_\pi; t, t_s), \end{aligned} \tag{16}$$

such that the form factors can be extracted by fitting the ratios themselves. A comparison between the two ratios for $h_\perp$ with injected momentum $|\mathbf{p}_\pi| = 0.5$ GeV is presented in Fig. 4 for a reference ensemble. In addition to the data, we also show the ground state results from the summation method as explained later in the text. We observe strong excited state contaminations in both ratio, with overall good agreement between the two approaches at different source-sink separations. On all the ensembles employed in this work we notice that the ratio $\mathcal{R}^{\rm II}$ is superior to $\mathcal{R}^{\rm I}$ in terms of statistical precision and it shows longer plateau regions.

3.3.1 Excited states contamination

In general, an exponential deterioration of the signal in three-point correlation functions is observed when increasing the source sink separation, thus forcing us to choose relatively short

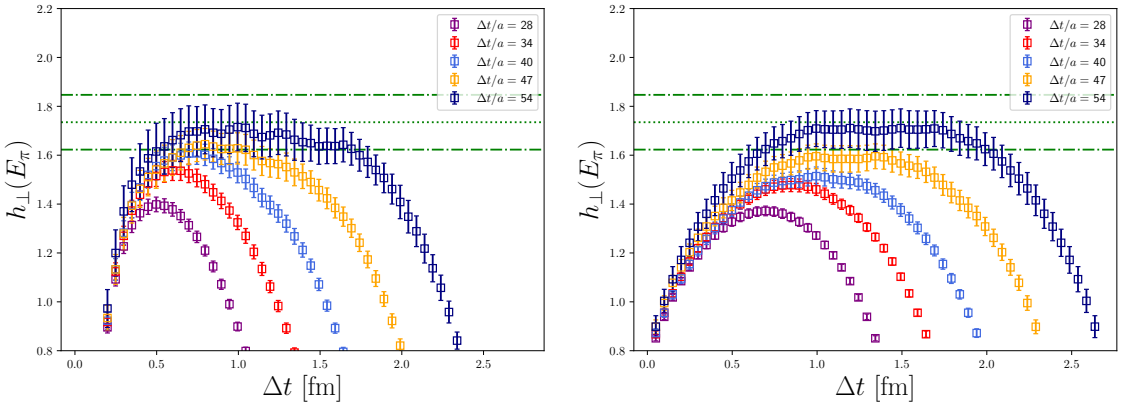

Figure 4: Overview of the ratios $\mathcal{R}^{\mathrm{I}}$ (*left*) and $\mathcal{R}^{\mathrm{II}}$ (*right*) for $h_\perp$ with injected momentum $|\mathbf{p}_\pi| = 0.5$ GeV, for an heavy-light meson in the region $m_h \sim 2.5 m_c$. Results are shown for the reference ensemble N300. The dashed horizontal values correspond to the ground state matrix element as extracted from the summation method using Eq. (18).

distances between operators in current lattice calculations of form factors observables. On the other hand, it cannot be ensured that contaminations from higher excited-states are sufficiently suppressed for the commonly available source-sink separations. In this context, the summation method [31–34] provides an alternative approach to improve the ground state convergence while controlling the systematics arising from excited states. Indeed, by computing for several values of the source-sink separation t_s the sum

$$S(t_s) = \sum_{t=0}^{t_s} \mathcal{R}^{\mathrm{I(II)}}, \tag{17}$$

we can extract the form factor of interest from the slope of a linear fit

$$S(t_s) \xrightarrow[t_s \gg 0]{} c + t_s h_{\perp(\parallel)}(m_\pi) + O(t_s \Delta e^{-t_s \Delta}), \tag{18}$$

with more strongly suppressed excited state contaminations with respect to $\mathcal{R}^{\mathrm{I(II)}}$. Here c is a fit parameter, while Δ denotes the gap between the ground and the first excited state of the mesons involved in the transition. An example of the fit in Eq. (18) to extract $h_\perp$ from the ratio $\mathcal{R}^{\mathrm{II}}$ is shown in Fig. 5 for our finest ensemble J500. We observe for all the ensembles employed in this work a well satisfied linear behaviour in $S(t_s)$.

4. Full computation of $B^{(\star)}$ leptonic decays

The $B^{(\star)}$ meson decay constants are extracted using Eq. (7) with the SSFs defined as in Eq. (8). The full strategy requires the usage of finite volume ensembles to compute the SSFs. These ensembles have been generated with Schrödinger Functional boundary conditions and with an action as given in [9] , where light quarks are kept massless. The finite volume boxes employed in this work range from $L_1 = 2L_0 \approx 0.5$ fm, where we measure relativistic quarks at the b scale, to $L_2 \approx 1.0$ fm, where both static and relativistic measurements are required to perform interpolations.

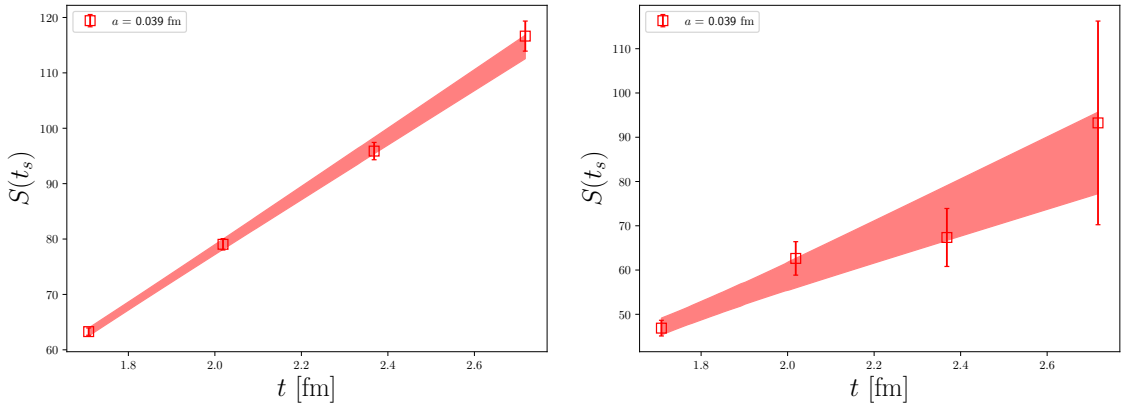

Figure 5: The summation method for $\mathcal{R}^{\mathrm{II}}$ to extract $h_\perp$ with injected momentum $|\mathbf{p}_\pi| = 0.5$ GeV (*left*) and $|\mathbf{p}_\pi| = 0.8$ GeV (*right*). Results are shown for the reference ensemble J500.

We refer to [4, 9, 35] for details on ensembles generation and the non-perturbative HQET-QCD matching. For the relativistic measurements in finite volume we cover a wide range of heavy quark masses, starting below the charm region and up to the b-quark mass. Discretisation effects in L_2, where both the volume and the lattice spacings are doubled, increase significantly above $m_b/2$.

4.1 Connecting L_2 to L_{CLS} and L_1 to $2L_1$

The starting point is the connection between the finite volume L_2 and the CLS ensembles listed in Tab. 1. In L_2, the tuning of the bare couplings to $\bar{g}^2(L_2) = 11.27$ for boxes of size $L_2/a = 12, \ldots, 32$ results in β values ranging in $3.4 \leq \beta \leq 3.97$, thus overlapping with CLS ensembles. Short interpolations in L/a to the CLS improved bare parameters $\tilde{g}_0^2$ [36, 37] are needed to match the two sets of data. Next, finite volume and infinite volume heavy-light matrix elements are computed in the range of the available bare heavy quark masses $a\tilde{m}_{q,h}$, and then interpolated to a common set of $\{y^{\mathrm{targ}}\}$ defined in the large volume. This allows to compute the lattice approximant of the relativistic SSFs as

$$\hat{\rho}_{A_0(\vec{V})}(u_2, y^{\mathrm{targ}}, a/L_2) = \Phi_{A_0(\vec{V})}(y) - \Phi_{A_0(\vec{V})}(u_2, y), \qquad \Phi_{A_0(\vec{V})}(u, y) = \ln\left(\frac{L_2^{3/2}}{\sqrt{2}}\hat{f}_{B^{(\star)}}\right), \quad (19)$$

where we chose $L_{\mathrm{ref}} = L_2$ to make observables dimensionless. The static SSFs are computed similarly, but no interpolation at fixed y^{targ} is required. Then, the continuum limit extrapolation to $\rho_{A_0(\vec{V})}(u, y) = \hat{\rho}_{A_0(\vec{V})}(u, y, 0)$ is performed with a linear dependence in a^2 and results are showed in Fig. 6. For the relativistic SSFs (left plot) we drop data with $am_h^{\mathrm{RGI}} > 0.8$, while in the static sector (right plot) we exclude the two coarsest lattice spacings. We note that in the static limit the presence of spin symmetry implies that pseudo-scalar and vector share the same SSFs $\sigma^{\mathrm{stat}}_{A_0} = \sigma^{\mathrm{stat}}_{\vec{V}}$ and $\rho^{\mathrm{stat}}_{A_0} = \rho^{\mathrm{stat}}_{\vec{V}}$. In addition, we stress out that the $O(a)$-improvement of $\hat{\rho}^{\mathrm{stat}}$, $\hat{\sigma}^{\mathrm{stat}}$ requires the knowledge of the improvement coefficient c_A^{stat}. The latter is not available for the Lüscher-Weisz gauge action, therefore we currently use the 1-loop determination of c_A^{stat} for the Wilson gauge action [38] with a 200% error.

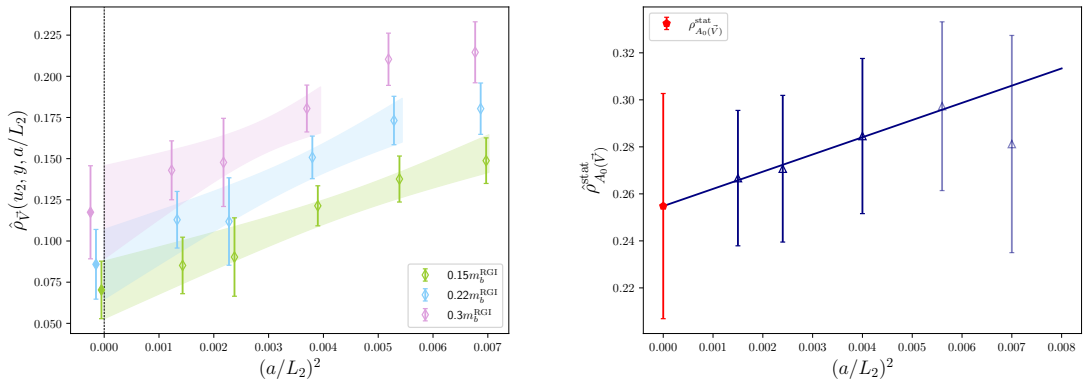

Figure 6: Continuum limit extrapolation for the relativistic vector (*left*) and static (*right*) SSFs connecting the volumes $L_2 \to \mathrm{CLS}$. In the relativistic sector we show a subset of the available heavy masses for a better readability.

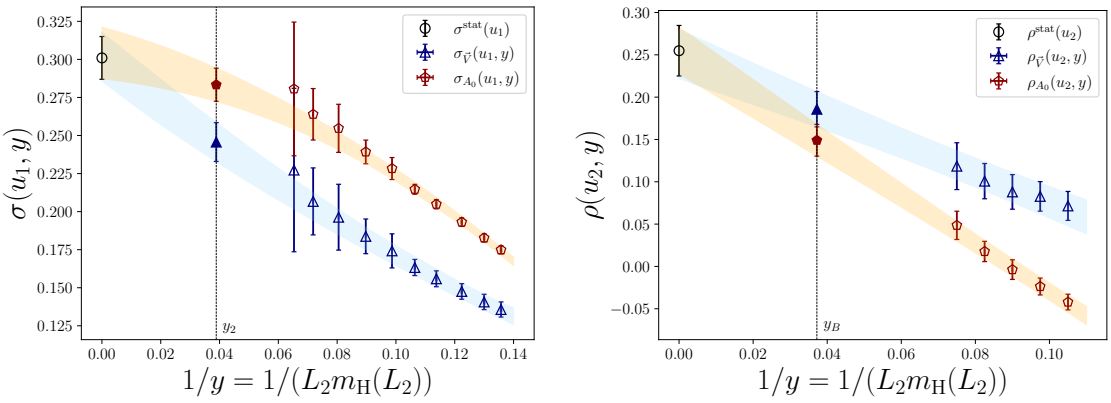

Figure 7: Interpolation to the target b-quark scale y_2 for the step $L_1 \to L_2$ (*left*) and y_B for the step $L_2 \to L_{\mathrm{CLS}}$ (*right*). Blu points correspond to the vector relativistic SSFs, while red ones denote the pseudo-scalar relativistic SSFs. The black circles correspond to the shared static SSFs σ^{stat} and ρ^{stat}.

The second step consists in computing the SSFs connecting $L_1 \to L_2 = 2L_1$, with the finite volume ensembles being generated at common values of the inverse coupling $\beta \in [3.65, 4.25]$. Having performed the relativistic measurements at equal values of the bare parameters in both finite volume ensembles, the only interpolations needed are to common $\{y^{\mathrm{targ}}\}$ but not in $am_{q,h}$. The finite-a SSFs are defined in analogy with Eq. (19), then the continuum limit is taken with a linear dependence in a^2. We observe also in this second step a good control of the cutoff effects while approaching the continuum for heavy quark masses $m_h \leq m_b/2$.

The strategy now consists in reaching the b-quark scale by interpolating static and relativistic SSFs in the continuum through the functional form [7]

$$\rho_{A_0(\vec{V})} = t_0 + t_1 y^{-1} + t_2 y^{-2}, \qquad \sigma_{A_0(\vec{V})} = c_0 + c_1 y^{-1} + c_2 y^{-2}, \tag{20}$$

where t_i, c_i are fit parameters.

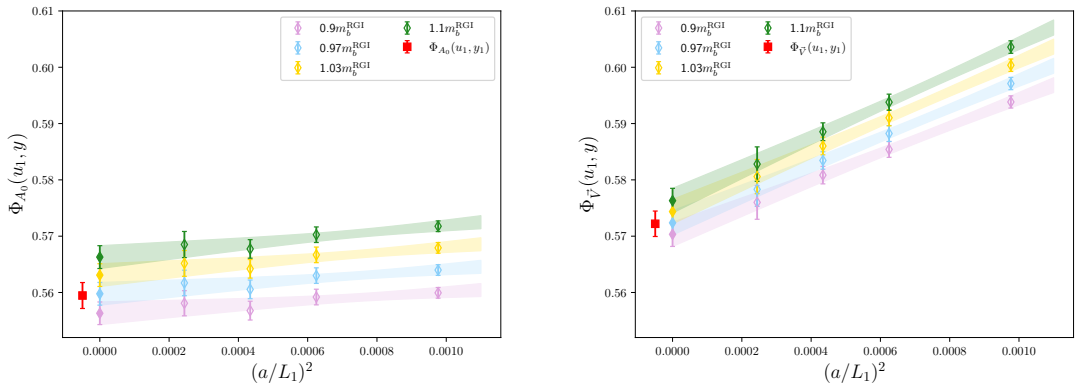

Figure 8: Continuum limit extrapolation for the pseudo-scalar (*left*) and vector (*right*) matrix elements in the finite volume L_1 at four different heavy-quark masses in the b-quark mass region. A fifth available lattice spacing is excluded from the fit. The filled red boxes show the interpolated value at the target y_1.

We determine the b-quark mass proxies from the large volume physical input using the flavour averaged combination of B and B_s meson masses [39], leading to $y_B = 26.87(18)$. This yields, together with the ρ_m SSF for the b-quark mass determined in [1] and Eq. (3) to a value of $y_2 = 25.72(19)$, used as proxy for the b-quark mass in the finite volumes L_1, $L_2 = 2L_1$. The interpolation to the target y_B, y_2 is shown in Fig. 7 for the pseudo-scalar and vector SSFs, from which we extract

$$\begin{aligned} \sigma_{A_0}(u_1, y_2) &= 0.283(11), \qquad & \sigma_{\vec{V}}(u_1, y_2) &= 0.246(13), \\ \rho_{A_0}(u_2, y_B) &= 0.149(18), \qquad & \rho_{\vec{V}}(u_2, y_B) &= 0.186(20), \end{aligned} \tag{21}$$

entering the chain in Eq. (7).

4.2 Relativistic QCD in L_1

The last step consists in determining the finite a approximant of $\Phi_{A_0(\vec{V})}(u_1, y)$ as defined in Eq. (6) in the finite volume $L_1 \approx 0.5$ fm. Here we reach very fine lattice spacings down to 0.008 fm, therefore allowing to simulate the relativistic b-quark mass without the need for a static computation. Having computed $\Phi_{A_0(\vec{V})}(u_1, y)$ for all the available L_1 boxes of size $L_1/a = 24, \ldots, 64$ we proceed with a continuum limit extrapolation, assuming a linear dependence on a^2. The results of the fit for the pseudo-scalar and vector matrix elements are shown in Fig. 8 for heavy quark masses in the range $0.9m_b < m_h < 1.1m_b$, where we observe a lattice spacing dependence well compatible with a^2. The continuum extrapolation is then followed by a linear interpolation in y to the physical point y_1. The latter is determined using Eq. (3) from the b-quark mass SSF σ_m computed in [1], leading to $y_1 = 24.66(19)$.

The results from the linear interpolation are shown in Fig. 8 with the full red squares. We now have all the pieces to extract the $B^{(\star)}$ meson decay constants from the step scaling chain in Eq. (7). Our preliminary results for the flavour averaged combination read

$$f_{\overline{B}} = 205.5(4.7)\ \text{MeV}, \qquad f_{\overline{B^\star}} = 207.0(5.4)\ \text{MeV}, \tag{22}$$

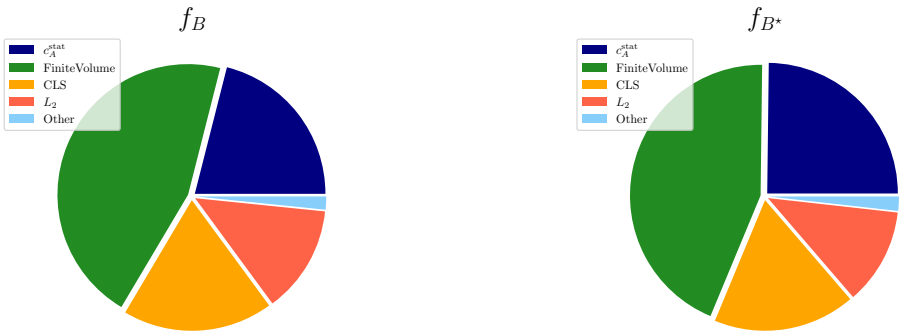

Figure 9: Summary of the error budget for the pseudo-scalar (*left*) and and vector (*right*) decay constants.

where we stress out that the input is the CLS $SU(3)$ symmetric point in the sea sector, and a careful study of the light quark mass dependence as approaching the physical point is still required. We refer to Fig. 9 for a summary of the error budget on the pseudo-scalar and vector decay constants. We observe that the dominant error source comes from the finite volume computation, where increased precision can be reached with additional statistics. The 200% error assigned to $c_A^{\rm stat}$ also play a significant role, and we expect this contribution to be substantially reduced once the improvement coefficient for the Lüscher-Weisz action is available.

5. Conclusion and Outlook

We have reviewed the strategy to combine static and relativistic results in the continuum first presented in [7] and extended beyond step scaling in volume from [2]. With respect to [1], where we discussed preliminary results for the b-quark mass and the $B^{(\star)}$ meson decay constants, here we presented our results in the relativistic large volume sector entering the full computation. We commented on the extraction of plateau averages from an Information Criteria for meson masses and leptonic matrix elements. In addition, we reported on the extraction of semi-leptonic amplitudes exploring different ratios between two- and three-point correlator functions. Then, we tested the summation method as a tool to parametrically suppress the excited states contaminations in form factors computations. Finally, we reviewed the extraction of the $B^{(\star)}$ meson decay constants detailing all the steps of our strategy and showing good control of the systematics involved in each phase of the computation.

Ongoing efforts are being made to extend our computation to lighter pion mass ensembles in the CLS sector, in order to reach the physical point also in this variable. Additional checks to infer the systematic uncertainties arising from the functional forms employed in continuum extrapolations and in the interpolations to the b-quark scale are being studied, together with different definitions of the finite volume observables. Ultimately, we plan to finalise the extraction of form factors for a precise determination of $B \to \pi \ell \nu$ semi-leptonic decays following the strategy pointed out in [7].

Acknowledgments

We thank Oliver Bär, Alessandro Barone, Alexander Broll and Andreas Jüttner for discussions. We acknowledge support from the EU projects EuroPLEx H2020-MSCAITN-2018-813942 (under grant agreement No. 813942), STRONG-2020 (No. 824093) and HiCoLat (No. 101106243), as well as from grants, PGC2018-094857-B-I00, PID2021-127526NB-I00, SEV-2016-0597, CEX2020-001007-S funded by MCIN/AEI, the Excellence Initiative of Aix-Marseille University - A*Midex (AMX-18-ACE-005), and by DFG, through the Research Training Group *"GRK 2149: Strong and Weak Interactions – from Hadrons to Dark Matter"* and the project "Rethinking Quantum Field Theory" (No. 417533893/GRK2575). J.H. wishes to thank the Yukawa Institute for Theoretical Physics, Kyoto University, for its hospitality. The authors gratefully acknowledge the Gauss Centre for Supercomputing e.V. (www.gauss-centre.eu) for funding this project by providing computing time on the GCS Supercomputer SuperMUC-NG at Leibniz Supercomputing Centre (www.lrz.de). We furthermore acknowledge the computer resources provided by the CIT of the University of Münster (PALMA-II HPC cluster) and by DESY Zeuthen (PAX cluster) and thank the staff of the computing centers for their support. We are grateful to our colleagues in the CLS initiative for producing the large-volume gauge field configuration ensembles used in this study.

References

[1] A. Conigli, J. Frison, P. Fritzsch et al., *PoS* **LATTICE2023** (2024) 237 [2312.10017].

[2] D. Guazzini, R. Sommer and N. Tantalo, *JHEP* **01** (2008) 076 [0710.2229].

[3] J. Heitger and R. Sommer, *Nucl. Phys. B Proc. Suppl.* **106** (2002) 358 [hep-lat/0110016].

[4] J. Heitger and R. Sommer, *JHEP* **02** (2004) 022 [hep-lat/0310035].

[5] M. Guagnelli, F. Palombi, R. Petronzio et al., *Phys. Lett. B* **546** (2002) 237 [hep-lat/0206023].

[6] G. M. de Divitiis, M. Guagnelli, R. Petronzio et al., *Nucl. Phys. B* **675** (2003) 309 [hep-lat/0305018].

[7] R. Sommer, A. Conigli, J. Frison et al., *PoS* **LATTICE2023** (2024) 268 [2312.09811].

[8] G. M. de Divitiis, R. Petronzio and N. Tantalo, *JHEP* **10** (2007) 062 [0707.0587].

[9] M. Dalla Brida, P. Fritzsch, T. Korzec et al., *Phys. Rev. D* **95** (2017) 014507 [1607.06423].

[10] P. Fritzsch, J. Heitger and S. Kuberski, *PoS* **LATTICE2018** (2018) 218 [1811.02591].

[11] I. Campos, P. Fritzsch, C. Pena et al., *Eur. Phys. J. C* **78** (2018) 387 [1802.05243].

[12] Y. Aoki et al., *Eur. Phys. J. C* **82** (2022) 869 [2111.09849].

[13] M. Bruno et al., *JHEP* **02** (2015) 043 [1411.3982].

[14] M. Bruno, T. Korzec and S. Schaefer, *Phys. Rev. D* **95** (2017) 074504 [1608.08900].

[15] D. Mohler, S. Schaefer and J. Simeth, *EPJ Web Conf.* **175** (2018) 02010 [1712.04884].

[16] D. Mohler and S. Schaefer, *Phys. Rev. D* **102** (2020) 074506 [2003.13359].

[17] M. Bruno, M. Dalla Brida, P. Fritzsch et al., *Phys. Rev. Lett.* **119** (2017) 102001 [1706.03821].

[18] B. Strassberger et al., *PoS* **LATTICE2021** (2022) 135 [2112.06696].

[19] A. Bussone, A. Conigli, J. Frison et al., *Eur. Phys. J. C* **84** (2024) 506 [2309.14154].

[20] J. Heitger, F. Joswig and S. Kuberski, *JHEP* **05** (2021) 288 [2101.02694].

[21] J. Frison, 2302.06550.

[22] M. Bruno and R. Sommer, *Comput. Phys. Commun.* **285** (2023) 108643 [2209.14188].

[23] W. I. Jay and E. T. Neil, *Phys. Rev. D* **103** (2021) 114502 [2008.01069].

[24] M. Dalla Brida, T. Korzec, S. Sint et al., *Eur. Phys. J. C* **79** (2019) 23 [1808.09236].

[25] Y. Taniguchi and A. Ukawa, *Phys. Rev. D* **58** (1998) 114503 [hep-lat/9806015].

[26] P. Fritzsch, *JHEP* **06** (2018) 015 [1805.07401].

[27] F. Bahr, D. Banerjee, F. Bernardoni et al., *Phys. Lett. B* **757** (2016) 473 [1601.04277].

[28] F. Bahr, D. Banerjee, F. Bernardoni et al., *Int. J. Mod. Phys. A* **34** (2019) 1950166 [1903.05870].

[29] J. M. Flynn, R. C. Hill, A. Jüttner et al., *Phys. Rev. D* **107** (2023) 114512 [2303.11280].

[30] J. M. Flynn, A. Jüttner, C. Sachrajda et al., *Journal of High Energy Physics* **2007** (2007) 016.

[31] L. Maiani, G. Martinelli, M. Paciello et al., *Nuclear Physics B* **293** (1987) 420.

[32] J. Bulava, M. Donnellan and R. Sommer, *JHEP* **01** (2012) 140 [1108.3774].

[33] S. Capitani, B. Knippschild, M. Della Morte et al., *PoS* **LATTICE2010** (2010) 147 [1011.1358].

[34] S. Capitani, M. Della Morte, G. von Hippel et al., *Phys. Rev. D* **86** (2012) 074502 [1205.0180].

[35] S. Kuberski, , *Standard Model parameters in the heavy quark sector from three-flavor lattice QCD*, Ph.D. thesis, "U. Münster", 2020.

[36] M. Lüscher, S. Sint, R. Sommer et al., *Nucl. Phys. B* **478** (1996) 365 [hep-lat/9605038].

[37] T. Bhattacharya, R. Gupta, W. Lee et al., *Phys. Rev. D* **73** (2006) 034504 [hep-lat/0511014].

[38] A. Grimbach, D. Guazzini, F. Knechtli et al., *JHEP* **03** (2008) 039 [0802.0862].

[39] P. A. Zyla et al., *PTEP* **2020** (2020) 083C01.